Received: 3 February 2022 | Revised: 16 September 2022 | Accepted: 21 September 2022

DOI: 10.1002/eqe.3756

RESEARCH ARTICLE

WILEY

Post-earthquake estimates of different ground motion intensity measures for the 2012 Emilia earthquake

Nicola Buratti | **Elena Simoni** | **Claudio Mazzotti**

DICAM - University of Bologna, Bologna, Italy

Correspondence
Nicola Buratti, DICAM - University of Bologna, Bologna, 40136, Italy.
Email: nicola.buratti@unibo.it

Abstract

Estimates of the earthquake ground motion intensity over a geographical area have multiple uses, that is, emergency management, civil protection and seismic fragility assessment. In particular, with reference to fragility assessment, it is of interest to have estimates of the values of different ground-motion intensity measures in order to correlate them with the observed damage. To this purpose, the present paper uses a procedure recently proposed in the literature to estimate the ground-motion intensity for the 2012 Emilia mainshocks, considering different ground motion intensity measures and directionality effects. Ground motion prediction equations based on different site effect models, and spatial correlation models are calibrated for the Emilia earthquakes. The paper discusses the accuracy of the shakemaps obtained using the different soil effect models considered and presents the obtained shakemaps as supplementary material. The procedure presented in the paper is aimed at providing ground motion intensity values for seismic fragility assessment and is not intended as a tool to estimate shakemaps for rapid emergency assessment.

KEYWORDS

Emilia earthquake, intensity measure, shakemap, spatial correlation

1 | INTRODUCTION

Shakemaps are quantitative estimates of the spatial distribution of the seismic ground-motion intensity in an area affected by an earthquake. These maps are a necessary tool for the formulation of damage scenarios and may be used either in the immediate aftermath of an earthquake to efficiently organise and distribute resources and personnel, or to implement preventive measures against strong earthquakes.

Shakemaps can be computed either for possible future earthquakes or for past events. In the second case, which is of interest for the present paper, recorded values of a ground-motion Intensity Measure (IM), obtained from Ground-Motion Recording Stations (GMRS), are combined with predictions made with a Ground-Motion Prediction Equation (GMPE). The classical approach used for computing shakemaps was proposed by Wald et al.;[1] it based on interpolating the data recorded by GMRSs, modified to take account local soil characteristics. The calculation also makes use of estimates of the shaking intensity provided by GMPEs. It is worth noticing that this method will not provide the IM recorded values at the sites of GMRSs. Recently, new calculation methods based on the normal multivariate distribution theory and on spatial correlation models have been proposed.[2,3] A GMPE is first adopted to estimate the values of the IM of interest at the points

of a regular grid; these values are then combined with recorded data, considering the spatial correlation of ground-motion intensity.[4] The influence of spatial correlation on IM predictions was studied by Jayaram and Baker,[5] while Goda and Atkinson investigated the same topic, with focus on Japanese earthquakes.[4] Esposito and Iervolino[6] evaluated the spatial correlation for Peak Ground Acceleration (PGA) and Peak Ground Velocity (PGV) from European datasets and discussed its application to regional seismic hazard analysis. Further studies are available for Iceland[7] and the Groningen area in the Netherlands.[8,9] These works however, mainly focus on spatial correlation models rather than on their actual role in the estimation of the IM distribution if the framework of shakemaps.

Up to date, shakemaps are automatically produced by the United States Geological Survey[10] in terms of Macroseismic Intensity, PGA, PGV and spectral acelerations at 0.3, 1.0 and 3.0 s. In Italy, shakemaps for the same IMs are instead produced by the Istituto Nazionale di Geofisica e Vulcanologia (INGV).[11] Until 2020, shakemaps in Italy were computed using the method proposed Wald et al.,[1] adapted to the Italian territory.[12] However, the maps computed by INGV before 2020, being automatically estimated right after the occurrence of earthquakes, relied on general GMPEs, used data from permanent GMRSs only and did not consider the spatial correlation of the ground-motion intensity. With reference to the 2012 Emilia earthquake, Braga et al.[13] analysed the reliability of the shakemaps produced by the INGV, concluding that, in some cases, their predictions did not correspond to the data recorded by the GMRSs. This difference was particularly evident for this earthquake because it is characterized by two mainshocks of similar magnitude, the first (Mw = 6.1) occurred on 20 May 2012 and the second (Mw = 6.0) on 29 May 2012, and after the first mainshock many temporary GMRSs were installed in the area; since their recordings were not used for computing the maps issued by INGV, it was possible to use their data to investigate the reliability of the shakemap predictions.

After 2020, INGV publishes shakemaps using a procedure similar to that adopted here, by means of the software Shakemap 4.0,[14,15] with a configuration that uses specific GMPEs and a $V_{s,30}$ map for Italy. Updated maps have been recomputed for past events as well, for the same IMs listed above, overcoming most of the aforementioned limitations. However, shakemaps for a restricted number of IMs, even if very useful for a rapid estimate of the severity of a seismic event, may become a limitation if they are to be used as a basis for fragility analysis.[16–18] The need for shakemaps in terms of different IMs is justified by a vast literature on the efficiency of IMs, which shows that the inelastic behaviour (and damage) of different types of structures correlates with different IMs,[19,20] and that IMs that do no not depend of the natural period of vibration of structures, such as PGA, even if widely used for developing observational vulnerability or fragility models,[18,21–24] have a very low efficiency.

The present paper presents shakemaps for the Emilia-Romagna 2012 main earthquakes in terms of several intensity measures, using the procedure proposed by[2] and.[3] They represent the first part of a project aimed at defining fragility models from observed damage data and are not intended as an alternative to the automatically computed shakemaps by INGV, which are a tool for obtaining rapid estimates of the ground motion intensity. First, attenuation relationships are derived using available ground motion recordings for the 2012 Emilia earthquakes. Several models are defined for a vast range of ground motion intensity measures, quantifying the amplification of site-effects with different empirical approaches. Along with event-specific attenuation relationships, empirical spatial correlation models are obtained, and both are then combined with ground motion recordings to calculate shakemaps. Maps are derived for the 20 May and 29 May earthquakes for all the considered IMs and their accuracy is evaluated by applying an iterative process in which IM values predicted by certain GMRS are randomly removed from the dataset and used to check the goodness of the shakemap prediction.

2 | ESTIMATION OF SHAKEMAPS BASED ON THE MULTIVARIATE NORMAL DISTRIBUTION THEORY

The procedure used in this work for computing shakemaps is derived from Bradley[2] and Worden et al.[3] Given a GMPE, the value of the logarithm of an IM induced by and earthquake e at a site of interest s can be assumed to have the following normal distribution

$$\log(IM_{e,s}) \sim N\left(\mu_{\log IM_{e,s}}\left(M_e, R_{e,s}, \theta_{e,s}\right), \sigma_{T,e,s}\left(M_e, R_{e,s}, \theta_{e,s}\right)\right) \quad (1)$$

where the $\mu_{\log IM_{e,s}}(M_e, R_{e,s}, \theta_{e,s})$ depends on earthquake magnitude M_e, source-to-site distance $R_{e,s}$ and, eventually, on other parameters $\theta_{e,s}$, as soil type, bedrock depth, style of faulting, etc., and $\sigma_{T,e,s}$ is the total standard deviation of the GMPE. Depending on the GMPE adopted, this latter parameter may either be constant or depend on some of the

parameters on which $\mu_{\log IM_{e,s}}$ depends. Within the framework adopted in the present paper the IM distribution defined by Equation (1) is named *unconditional*. In the present paper log(·) indicates base 10 logarithms.

Considering an $IM_{e,r}$ value obtained from a GMRS *r* for an earthquake *e* it is possible to write

$$\log(IM_{e,r}) = \mu_{\log IM_{e,r}}\left(M_e, R_{e,r}, \theta_{e,r}\right) + \zeta_{e,r} \tag{2}$$

where $\zeta_{e,r}$ is the total residual, which can be decomposed into its *between*- and *within*-event components, δ_{B_e} and $\delta_{W_{es}}$, also named inter-event and intra-event components, respectively,

$$\zeta_{e,r} = \delta_{B_e} + \delta_{W_{e,r}}. \tag{3}$$

The between-event component is common to all the GMRSs, and it is associated to the earthquake, that is it represents the systematic difference between the residuals associated to ground-motions produced by different earthquakes. Instead, the within-event component varies from site to site, and describes the variability within the ground-motion recordings of the same earthquake. Within-event residuals have been demonstrated to be spatially correlated as a consequence of GMRS sites sharing similarities among path and sites effects; this correlation is inversely proportional to the separation distance.[2,4,5] Both the between- and within-event residuals are assumed to be samples from normally distributed random variables with null mean and standard deviations σ_B and $\sigma_{W,e,s}$ respectively,

$$\delta_{B_e} \sim N\left(0, \sigma_B\right) \tag{4}$$

$$\delta_{W_{e,r}} \sim N\left(0, \sigma_{W,e,r}\right). \tag{5}$$

According to Bradley[2] and Worden et al.,[3] a multivariate normal distribution is introduced to describe the joint distribution of the logarithm of the ground-motion IM values at different sites produced by a given earthquake. Furthermore, a spatial correlation model is used to estimate the distribution of the ground-motion IM conditional to the values recorded at locations of a set of GMRSs. Given *n* values of the IM, recorded by *n* GMRSs, the value of the between-event residual, $\delta_{B,e}$, is calculated as[2]

$$\delta_{B,e} = \frac{1^T \boldsymbol{\Sigma}^{-1}_{GMRS-GMRS} \boldsymbol{\zeta}}{\left(1/\sigma_B^2\right) + 1^T \boldsymbol{\Sigma}^{-1}_{GMRS-GMRS} 1} \tag{6}$$

where 1 is a *n* x 1 vector, $\boldsymbol{\zeta}$ is a *n* x 1 vector containing the total residual at each of the *n* GMRSs, computed by subtracting the IM values predicted by a GMPE (Equation 1) from the measurements of the GMRSs, while $\boldsymbol{\Sigma}_{GMRS-GMRS}$ is a *n* x *n* variance-covariance matrix for the within-event residuals. The general component $(\boldsymbol{\Sigma}_{GMRS-GMRS})_{i,j}$ of this matrix represents the correlation between the within-event residuals at the *i*-th and at the *j*-th GMRSs and is defined as[2]

$$(\Sigma_{GMRS-GMRS})_{i,j} = \rho_{i,j}\sigma_{W,e,i}\sigma_{W,e,j} \tag{7}$$

being $\rho_{i,j}$ the spatial correlation between the within-event residuals at the two GMRSs under consideration and $\sigma_{W,e,i}$ and $\sigma_{W,e,j}$ their within-event standard deviations as defined by a GMPE. Indicating with $\log(IM_{e,s})$ the *unconditional* ground motion intensity predicted by a GMPE at a site *s* and with $\log(\boldsymbol{IM}_{eSMS})$ the *n* x 1 vector of measured IM values at the locations *n* GMRSs, the *conditional* distribution of the IM at the site *s* given the measurement of the GMRSs is assumed to have the following mean value[2]

$$\mu_{\log(IM_{e,s})|\,\log(\boldsymbol{IM}_{e,GMRS})} = \mu_{\log(IM_{e,s})} + \boldsymbol{\Sigma}_{s-GMRS}\boldsymbol{\Sigma}^{-1}_{GMRS-GMRS}\boldsymbol{\delta}_{W_{e,r}} + \delta_{B_e} \tag{8}$$

where Σ_{s-GMRS} is a 1 x *n* variance-covariance matrix describing the correlation between the ground motion intensity at the site s and at the sites of the GMRS, computed as[2]

$$(\Sigma_{s-GMRS})_{1,r} = \rho_{s,r}\sigma_{W,e,s}\sigma_{W,e,r} \tag{9}$$

TABLE 1 Earthquakes from the Emilia 2012 sequence used for deriving GMPE and spatial correlation models

Earthquake ID	Date	Municipality	Latitude [°]	Longitude [°]	Depth [km]	M_W [-]	GMRSs used
IT-2012-0008	2012-05-20 02:03:50	Finale Emilia	44.89550	11.26350	9.50	6.1	82
IT-2012-0011	2012-05-29 07:00:02	Medolla	44.84170	11.06570	8.07	6.0	113
IT-2012-0010	2012-05-29 10:55:56	Cavezzo	44.86520	10.97950	4.35	5.5	95
IT-2012-0032	2012-05-29 11:00:22	San Possidonio	44.86600	10.97630	7.20	5.5	35

Latitude and longitude are referred to the epicentre while the depth is that of the hypocentre. Data were obtained from the ITACA database.[29]

and $\delta_{W_{e,r}}$ is computed using Equations (1), (2) and (5). The variance of the *conditional* IM distribution at site s is computed as[2]

$$\sigma^2_{\log(IM_{e,s})|\log(IM_{e,GMRS})} = \sigma^2_{W,e,s} - \boldsymbol{\Sigma}_{s-GMRS}\boldsymbol{\Sigma}^{-1}_{GMRS-GMRS}\boldsymbol{\Sigma}_{GMRS-s} \tag{10}$$

In[2] the uncertainty in the between-event residual is included into the conditional variance of ground motions, as the within- and between-event residuals are no longer independent when conditioned upon GMRS data. This is neglected in the present paper because, as discussed in Section 3, the attenuation models used have very small between-event uncertainties. An improvement on this conditioning has recently been proposed by Engler et al.[25]

It should be noticed that, according to the approach adopted, the conditional IM distribution at the location of one of the GMRSs has a mean value corresponding the recorded IM value and zero variance. Therefore, the present model does not consider any measurement error in GMRSs. If Equations (8) and (10) are applied to a grid of sites a shakemap is obtained, but they may be applied also to irregularly spaced points, for instance to estimate IM values at the locations of a set of buildings. When IM values are calculated on regular grid, the stations will generally never be coincident with the grid mesh, therefore at their location the prediction error will not be zero, since the IM values will be obtained by interpolation of the values at the neighbouring grid points.

3 | ATTENUATION MODELS FOR THE 2012 EMILIA EARTHQUAKE

As discussed in Section 2, in order to derive shakemaps for a certain ground-motion IM a GMPE and a spatial correlation model are needed. In the literature there are models for some of the IMs that are considered in the present study[26–28] but we have chosen to fit new models using data from the 2012 Emilia earthquake for the following reasons: i) consider IMs for which there are no attenuation or spatial correlation models available; ii) achieve an high level of consistency among the different IM GMPEs, using the same dataset for all the attenuation models and the same functional form; iii) consider directionality of ground motions in order to define orientation-independent values of the IMs; iv) consider regional geological data in the calibration of the models (e.g. bedrock depth, $V_{s,30}$); v) achieve an high goodness of fit on the IM values produced by Emilia earthquake; vi) obtain within-event standard deviations specific for the Emilia 2012 earthquake. Clearly, the models presented in the present work are specific to the 2012 Emilia earthquake and may not be suited to predict the effects of other earthquakes. This section describes the derivation of the aforementioned models and the processing of recorded accelerograms.

3.1 | Ground motion recordings

During the end of May 2012, the Emilia-Romagna region, in northern Italy, was affected by a series of moderate intensity seismic events, which have mainly interested the provinces of Modena, Ferrara and Bologna. The strongest shocks struck on 20 and 29 May and had moment magnitudes of 6.1 and 6.0, respectively.[29] In the present work, only earthquakes of the 2012 Emilia sequence with $M_W \geq 5$ and with information about the geometry of the rupture plane were considered, for a total of four events (Table 1). Figure 1 shows the location of their epicentres and the surface projections of their rupture planes. Earthquake and ground-motion data and rupture planes were obtained from the Italian

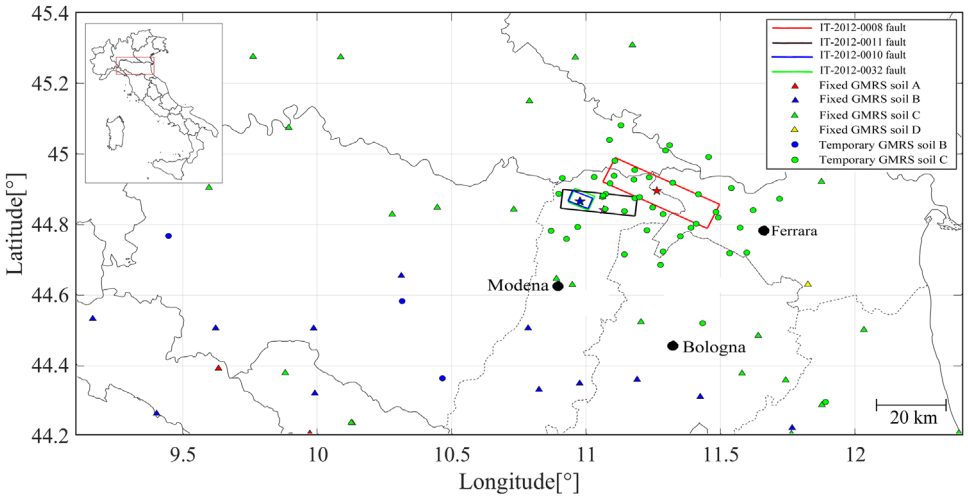

FIGURE 1 Finite faults from the Emilia 2012 earthquakes. Temporary and fixed stations are coloured according to the associated soil class.[16] Damage from these events affected the three provinces of Modena, Bologna and Ferrara.

Accelerometric Archive (ITACA),[29] this archive contains six events with $M_w \geq 5$ but for two of them the geometry of the rupture planes was not available when the data was downloaded and were not used. It is worth noticing that the number of GMRSs in the epicentral area is much higher for the events after the 20th May, because many temporary GMRSs were installed after the first mainshock. It is noted that the number of GMRSs reported in Table 1 accounts only for those stations for which data on $V_{s,30}$ were available, because this parameter was needed to calibrate ground motion attenuation relationships, as explained in the following. Furthermore, given the purpose of the paper, only stations at distances shorter that 200 km were used. All the ground acceleration recordings used are filtered according to the procedure described in.[30]

3.2 | Ground motion IMs and directionality

In this work, the following ground-motion IMs have been considered:

- Peak Ground Acceleration (PGA)

$$PGA = \max\left(|a\left(t\right)|\right) \tag{11}$$

  $a(t)$ where *a(t)* is the ground acceleration;
- pseudo-spectra accelerations at the period T_1

$$Sa\left(T_1\right) \tag{12}$$

  with T_1 equal to either 0.3, 0.7 or 1.5 s;
- the average spectral acceleration in the range 0.1 s - 0.5 s

$$Sa_{0.1-0.5} = \left(\sum_{T\geq 0.1s}^{T\leq 0.5s} Sa\left(T_i\right)\right)/n \tag{13}$$

  where T_i is the i-th period at which the pseudo-spectral acceleration is computed;

TABLE 2 Period spacing ΔT used in the different period intervals [T_L, T_U] considered for computing elastic spectra

T_L [s]	0.025	0.05	0.11	0.22	0.55	1.1	4.2
T_U [s]	0.025	0.1	0.2	0.5	1.0	4.0	10
ΔT [s]	–	0.005	0.01	0.02	0.05	0.1	0.2

– Housner's spectral intensity[31]

$$SI_H = \int_{0.1}^{2.5} Sv(T)\,dT \tag{14}$$

where Sv(T) is the pseudo-spectral velocity;

– the geometric mean of the pseudo-spectral acceleration in the range of periods T_1-2.0T_1[32]

$$Sa_{avg,T1}(T_1,\cdots,2T_1) = \left(\prod_{i=1}^{n} Sa(T_i)\right)^{1/n} \tag{15}$$

– the IM proposed by Bojórquez and Iervolino[33]

$$I_{Np,T1} = Sa(T_1)\left[\frac{Sa_{avg}(T_1,\cdots,2T_1)}{Sa(T_1)}\right]^{0.4} \tag{16}$$

– the IM proposed by Cordova[34]

$$I_{Mc,T1} = \sqrt{Sa(T_1)}\sqrt{Sa(2T_1)} \tag{17}$$

– the IM proposed by Kappos[35]

$$SI_{H,K} = \int_{0.8T_1}^{1.2T_1} Sv(T)\,dT \tag{18}$$

– the IM proposed by Matsumura[36]

$$SI_M = \int_{T_1}^{2T_1} Sv(T)\,dT \tag{19}$$

The parameter T_1 in Equations (12)-(19) was set to either 0.3 or 0.7 or 1.5 s, in order to represent short-, medium- and long-period structures. All IMs based on response spectra were computed considering a damping ratio of 0.05. All the IMs considered are evaluated starting from discrete elastic spectra computed at the periods listed in Table 2. The IMs considered were defined based on previous studies on their efficiency in predicting the inelastic behaviour of different types of structures.[19]

The vertical component of ground-motions was not considered in this work. As for the horizontal components, directivity effects were taken into account by means of the methodology proposed by Boore et al.[37] In particular, each IM was computed for different horizontal directions, considering 5 degrees increments. As an example, Figure 2 shows the PGA, in different horizontal directions at the MRN GMRS in Mirandola, for all the considered earthquakes. The minimum (0% percentile), median (50% percentile) and maximum (100% percentile) values each IM among those associated to the different horizontal directions were used to derive GMPEs. According to Boore et al.,[37] these values are named IM_{ROTD0},

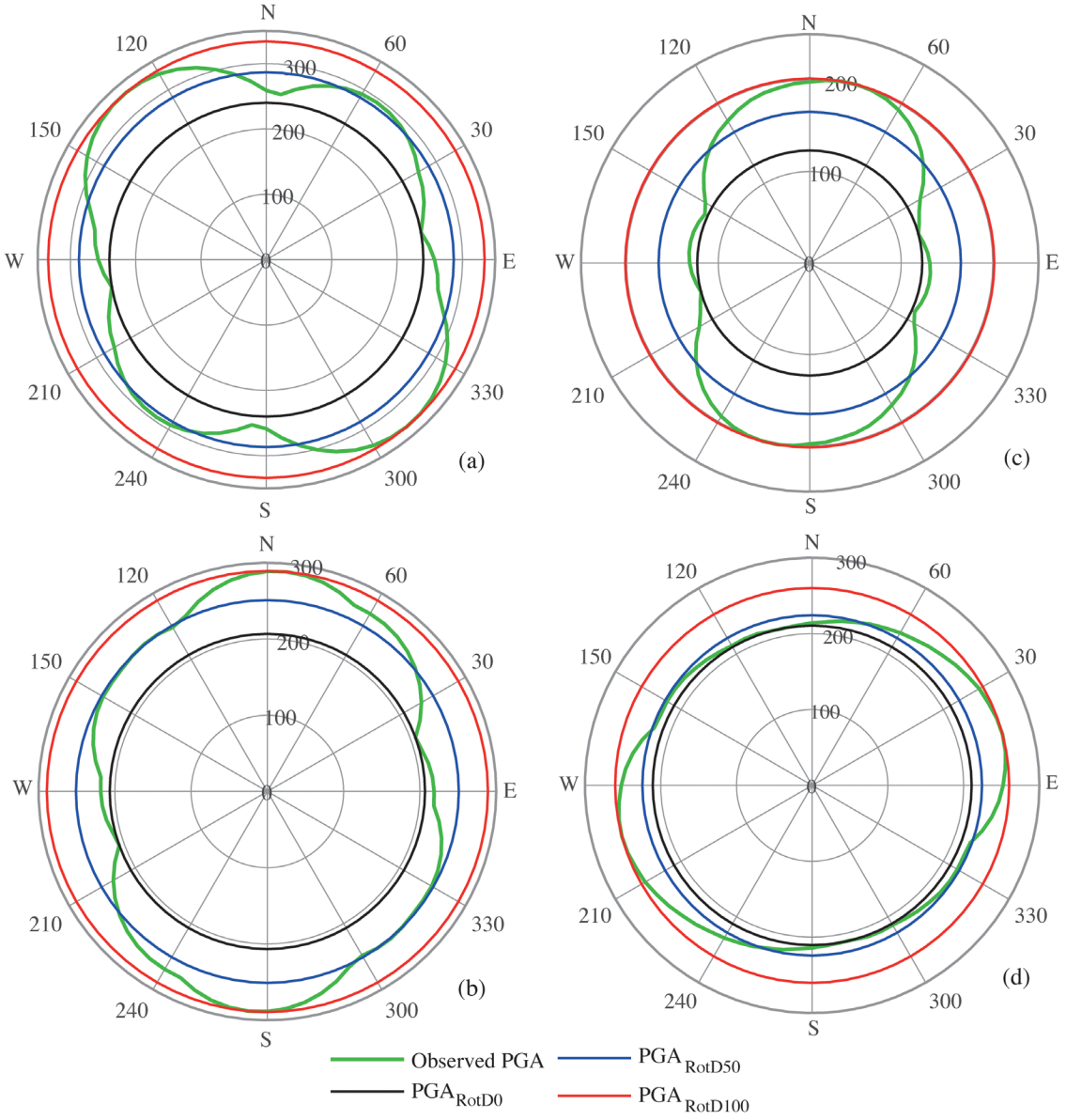

FIGURE 2 PGA in different horizontal directions at the MRN GMRS for the: (A) 20th May main event IT-2012-0008, (B) 29th May main event, IT-2012-0011, (C) IT-2012-0010 and (D) IT-2012-0032 29th May aftershock events. For each plot maximum ($PGA_{RotD100}$), median (PGA_{RotD50}) and minimum (PGA_{RotD0}) are shown. See Table 1 for the event codes.

IM_{ROTD50} and $IM_{RotD100}$, respectively. It should be noticed that when considering orientation-independent IMs, as done in the present study, it is not possible to use GMPEs for spectral accelerations at specific periods (i.e. $Sa(T_i)$) in order to define the attenuation of the geometric mean of spectral accelerations in a given range of periods, because the minimum, median and maximum functions involved in the calculation of IM_{ROTD0}, IM_{ROTD50} and $IM_{RotD100}$ are non-linear.

3.3 | Geological data for the area of study

3.3.1 | Bedrock depth

Shakemaps and the GMPEs they rely on must describe site effects. In this study, data on the shear wave velocity in the uppermost 30 m, $V_{s,303}$ and on the depth of the bedrock have been used to this purpose.

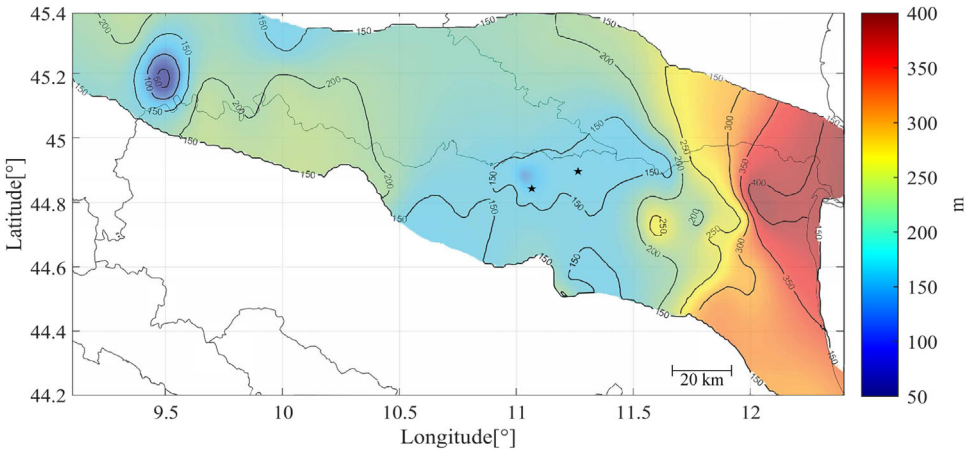

FIGURE 3 Bedrock depth map, covering the areas affected by the 2012 Emilia earthquakes. Different range of colours and black lines contour areas characterised by similarities in bedrock depth values. Epicentres for the 20th and 29th main events are marked with stars.

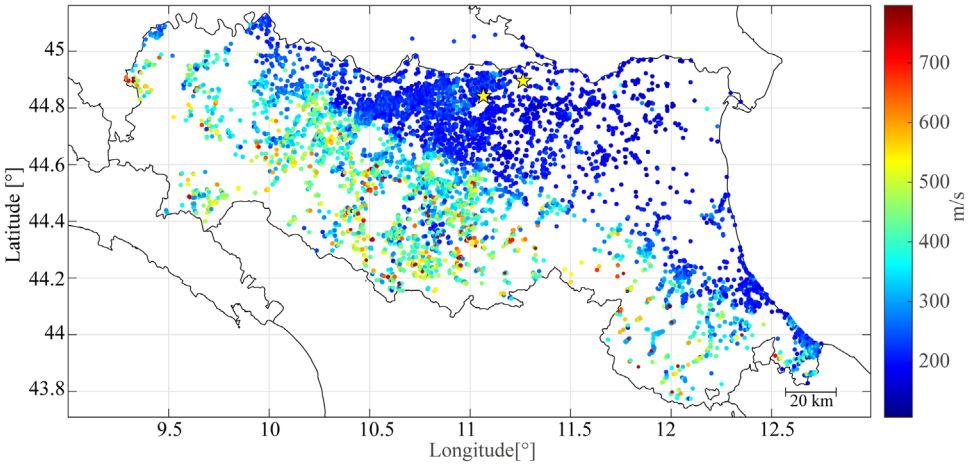

FIGURE 4 $V_{S,30}$ profiles investigation sites in the Emilia-Romagna region. $V_{S,30}$ values associated with each survey have been divided into soil categories according to the Italian building code (NTC2018) prescriptions, reported in Table 3.[39] It can be observed that the most prevalent soil category in the epicentral area is type C. Epicentres for the 20th and 29th main events are marked with stars.

After the 2012 events, Mascandola et al.,[38] have produced a detailed bedrock depth map for the area most severely affected by the earthquakes (Figure 3) using passive seismic prospecting methods based on ambient vibration measurements. This map is provided as a high-quality image with embedded georeferencing information. Therefore, through direct linear interpolation of the data points it is possible to obtain bedrock depth values all over the area investigated. In Figure 3, contour lines mark lines with constant bedrock depth, while its variation over the territory is mapped by means of a colour scale. The maps show that in the area closer to epicentres (stars) the bedrock depth is almost uniform with a depth of about 150 m.

Concerning data on $V_{s,30}$ values, the Emilia-Romagna region has collected the outputs of all the micro-zonation studies carried out since 2012,[40] for a total of 9406 data points (Figure 4). In the epicentral area $V_{s,30}$ values range from around 200 m/s up to slightly lower than 400 m/s, which according to the Italian Building Code correspond to soil class C (180 m/s < $V_{s,30}$ < 360 m/s).

Since these $V_{S,30}$ profiles, are point based and have an irregular spatial distribution, a proper continuum interpolation model must be defined, in order to integrate these data in the shakemap estimation procedure. Two different approaches were used to this aim; the first method is directly derived from the approach described for computing shakemaps, while the second is based on a universal kriging.[41]

Concerning the first method, the procedure described in Section 2 is used in order to estimate the distribution of $\log_{10}(V_{s,30})$ *conditional* to the values measured at the locations of the points depicted in Figure 4. To this purpose, the

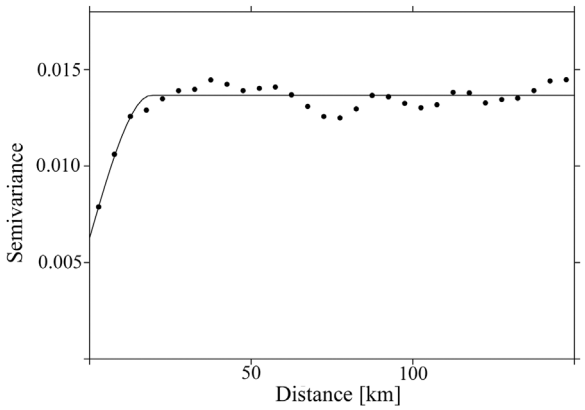

FIGURE 5 Empirical spherical semi-variogram fitted to residuals from the $V_{s,30}$ linear regression.

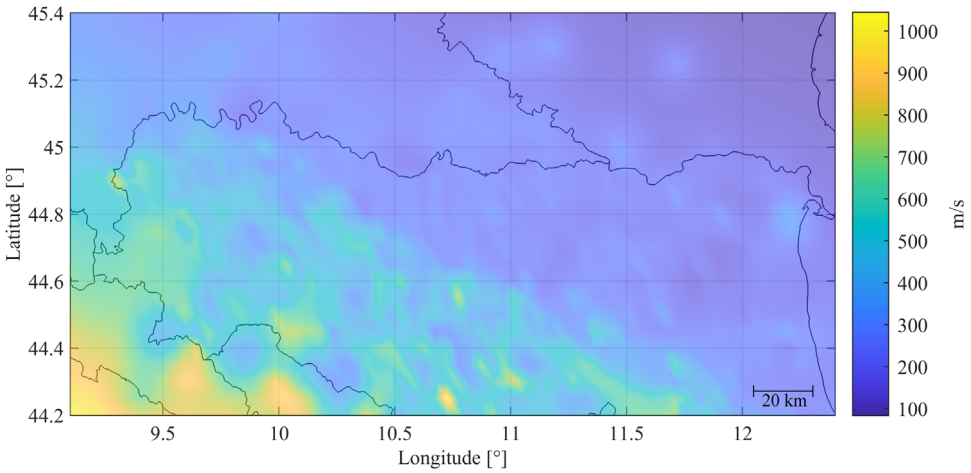

FIGURE 6 Conditional $V_{s,30}$ distribution. This approach relies on a linear regression model calibrated on available data and a spatial correlation model.

points at which $V_{s,30}$ is available are considered here similarly to how GMRSs were used in Section 2 to estimate the conditional distribution of log(IM). In place of a GMPE a linear regression model was defined for describing the dependency of the measured $V_{s,30}$ values on geographical coordinates. The functional form adopted is

$$\log\left(V_{S,30}\right) = c_1 + c_2 \cdot \overline{UTM_x} + c_3 \cdot \overline{UTM_y} + \varepsilon \tag{20}$$

where $\overline{UTM_x}$ and $\overline{UTM_y}$ are the planar coordinates of each datapoint and ε is a normal error term. The origin of the coordinate system used to measure these distances was set on the geographical centroid of the point data. Finally, a spherical spatial correlation model was defined by analysing the residuals of the linear regression model in Equation (20). The employed semi-variogram model is shown in Figure 5, while the *conditioned* distribution of $\log_{10}(V_{s,30})$, obtained as described in Section 2, is reported in Figure 6.

The second approach, instead, adopts a *universal kriging* model, that allows the prediction of a variable accounting for a spatial correlation model and a trend characterising the observations. Universal kriging[42] generally combines trend surface analysis with ordinary kriging so that trends in the observations can be accounted for. The adopted trend is that described by Equation (20) and the spatial correlation model is the same as that derived for the first method. The $V_{s,30}$ map obtained with kriging interpolation is presented in Figure 7.

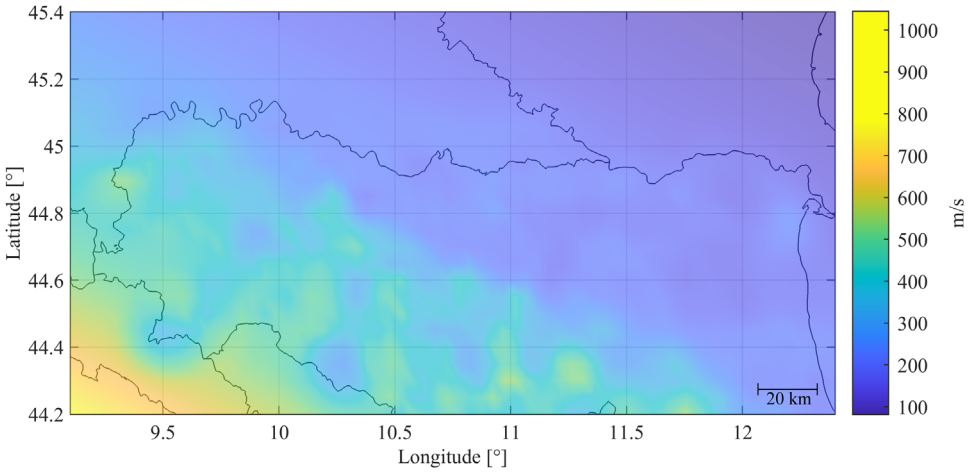

FIGURE 7 $V_{s,30}$ map derived kriging interpolation, where the spatial trend of the data is assumed to be described by

3.4 | GMPE functional form

As the final objective of this work is to derive a strictly regional tool and given that, up to date, there are no GMPEs for all the IMs under consideration with reference to the Emilia-Romagna region, specific attenuation relationships have been defined. The functional form adopted is

$$\log(IM) = c_1 + c_2 \cdot M_w + c_3 \cdot \log\left(\sqrt{R^2 + c_4^2}\right) + c_5 \cdot \log(R + 25) + SE + \sigma_W \varepsilon_w + \sigma_B \varepsilon_b \tag{21}$$

where log*(IM)* is the base 10 logarithm of the intensity measure under consideration, M_w is the moment magnitude of the earthquake, R is the Joyner-Boore distance in km, SE is a term representing site effects, while ε_w and ε_b are standard normal random variables, accounting for the within- and between-event errors, respectively. In this model the within-event standard deviation is assumed as constant, given the limited number of earthquakes considered and their reduced magnitude range.

Site conditions are often included in GMPEs through $V_{s,30}$ values or soil classifications derived from $V_{s,30}$.[43] Recently, some authors have tried to consider the effect of deep geological; Chiou and Youngs[44,45] for example, have considered in addition to $V_{s,30}$ the depth to the 1 km/s velocity horizon, $Z_{1,0}$. In this work four different formulations for the site effect term in the GMPE have been considered. The first introduces a linear term proportional to $\log(V_{s,30})$

$$SF = c_6 \cdot \log(V_{s,30}) \tag{22}$$

the second is based on the soil classification adopted by the Italian national building code

$$SF = c_6 \cdot S_B + c_7 \cdot S_C + c_8 \cdot S_D \tag{23}$$

where S_B is dummy variable equal to 1 for soil class B and 0 otherwise, S_C is a dummy variable equal to 1 for soil class C and 0 otherwise and S_D is dummy variable equal to 1 for soil class D and 0 otherwise. Soil classes are defined based on the intervals reported in Table 3.

The third approach is derived from the non-linear site effect model proposed by the Italian building code for defining elastic spectra on different soil classes[39]

$$SF = f\left(Sa_{0.1-0.5,A}, V_{s,30}\right) \tag{24}$$

TABLE 3 $V_{s,30}$ ranges for each soil class according to the Italian Building Code[39]

Soil class	$V_{s,30}$ range
A	800 m/s
B	360 m/s - 800 m/s
C	180 m/s - 360 m/s and bedrock deeper than 30 m
D	100 m/s - 180 m/s and bedrock deeper than 30 m
E	100 m/s - 360 m/s and bedrock shallower than 30 m

where $f(Sa_{0.1-0.5,A}, V_{s,30})$ is defined as

$$f\left(Sa_{0.1-0.5,A}, V_{s,30}\right) = \begin{cases} 1 & \text{for soil class A} \\ 1.0 \le 1.4 - 0.4\dfrac{Sa_{0.1-0.5,A}}{g} \le 1.2 & \text{for soil class B} \\ 1.0 \le 1.7 - 0.6\dfrac{Sa_{0.1-0.5,A}}{g} \le 1.5 & \text{for soil class C} \\ 0.9 \le 2.4 - 1.5\dfrac{Sa_{0.1-0.5,A}}{g} \le 1.8 & \text{for soil class D} \\ 1.0 \le 2.0 - 1.1\dfrac{Sa_{0.1-0.5,A}}{g} \le 1.6 & \text{for soil class E} \end{cases} \tag{25}$$

and $Sa_{0.1-0.5,A}$ is the average spectra acceleration in the range 0.1 – 0.5 s on soil class A, and the soil classes are defined according to Table 3.

Given a ground-motion recording on a soil class SC different from A its average spectral acceleration in the range 0.1 –0.5 s is computed ($Sa_{0.1-0.5,SC}$) and the value of the site effect function is found by solving the equation

$$Sa_{0.1-0.5,SC} = f\left(Sa_{0.1-0.5,A}, V_{s,30}\right) Sa_{0.1-0.5,A} \tag{26}$$

The so obtained site amplification coefficient is then applied to all the intensity measures, being all based on either pseudo-acceleration or pseudo-velocity response spectra.

The fourth approach is based on the site effect model proposed by c

$$SF = f\left(IM_{bedrock}, V_{s,30}, Z_{1,0}\right) \tag{27}$$

where $f(IM_{bedrock}, V_{s,30}, Z_{1,0})$ is defined as

$$\begin{aligned} f\left(IM_{bedrock}, V_{s,30}, Z_{1,0}\right) = {} & \varphi_1 \min\left(ln\left(\frac{V_{s,30}}{1130}\right), 0\right) + \varphi_2\left(e^{\varphi_3\left(\min\left(V_{s,30},1130\right)-360\right)} - e^{\varphi_3(1130-360)}\right) \ln\left(\frac{IM_{bedrock}+\varphi_4}{\varphi_4}\right) \\ & + \varphi_5\left(1 - e^{-\Delta Z_{1,0}/\varphi_6}\right) \end{aligned} \tag{28}$$

with

$$\Delta Z_{1,0} = \begin{cases} Z_{1,0} - \exp\left(\dfrac{-7.15}{4} \ln\left(\dfrac{V_{s,30}^4 + 571^4}{1360^4 + 571^4}\right)\right) & \text{where } Z_{1,0} \text{ is known} \\ 0 & \text{otherwise} \end{cases} \tag{29}$$

Estimates of the regression coefficients φ_i in Equations (29) and (30), are provided by[45] but are available only for a limited number of IMs, namely the PGA, PGV, PGD and spectral accelerations for different periods ranging from 0.01 to 10 s. Therefore, this approach could not be implemented for all the ground motion intensity measures evaluated in this study. However, coefficients have been derived for a few additional IMs that are directly obtained from the spectral acceleration, such as Sa_{avg}, Sa_{T1} and $Sa_{0.1-0.5}$ using the formulas shown in Section 3. The site effect term was evaluated for

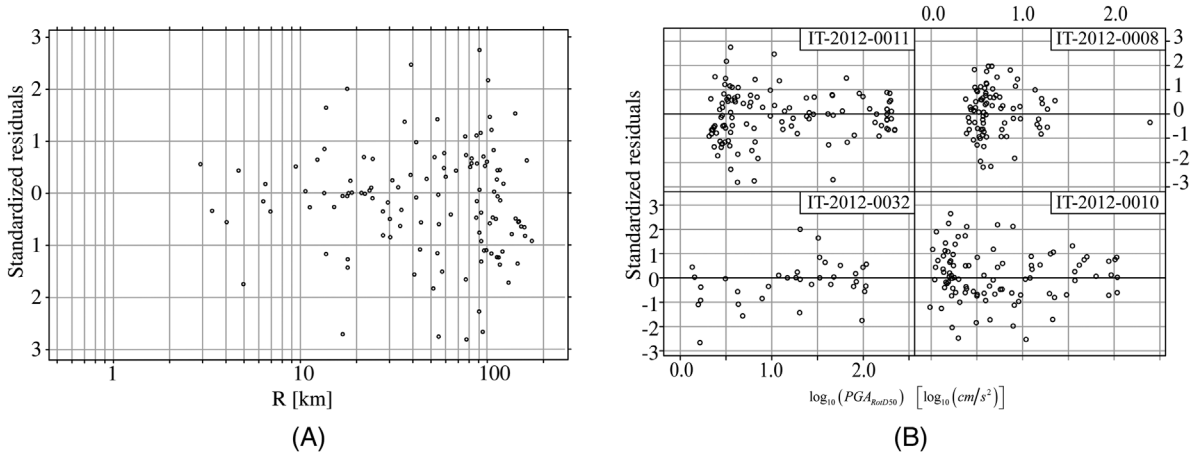

FIGURE 8 Residuals from the regression analysis for PGA_{RotD50} and AT3 model against Joyner Boore distance (A) and against fitted values, grouped for different the different earthquakes considered (B).

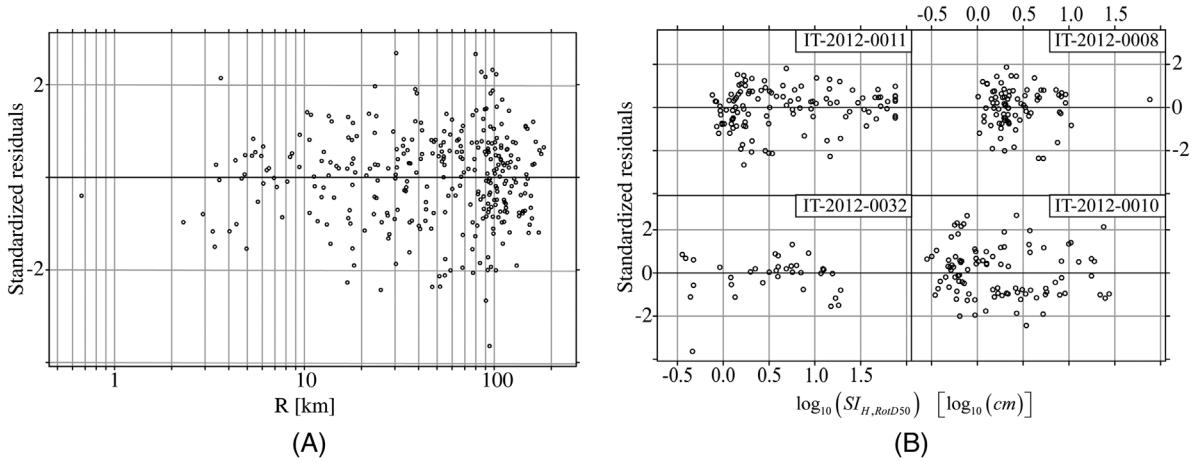

FIGURE 9 Residuals from the regression analysis for SIH_{RotD50} and AT3 model against Joyner Boore distance (A) and against fitted values, grouped for the different earthquakes considered (B).

each available ground motion recording station, noting that each station is assigned a $V_{s,30}$ value, while $\Delta Z_{1,0}$ is computed according to Equation (29).

The $V_{s,30}$ and the $Z_{1.0}$ values used in the development of GMPEs were not available for all the GMRSs. For stations located inside the Emilia-Romagna region without data on either $V_{s,30}$ or $Z_{1.0,}$ estimates from the models described in Section 3 were used. Clearly, these models cannot provide estimates for GMRSs outside the Emilia region, therefore, stations not covered by the models presented in Section 3, for which $V_{s,30}$ values were not provided, were discarded, whereas stations that did not have $Z_{1.0}$ were kept using $\Delta Z_{1,0} = 0$ according to Equation (30). Combining Equation (21) with one of the four different site effect models four different GMPEs can be obtained. These will be referred to as *AT1, AT2, AT3* and *AT4*.

The values of the regression coefficients of the GMPE in Equation (21) – and (22) and (23) for the models AT1 and AT2– which can be classified as a non-linear mixed effects statistical model, were estimated by means of nonlinear regression, using the software R.[46] Various tests were carried out during the regression analysis, in order to check the quality of the models, analysing the normality of the residuals and the absence of trends between the latter and either the covariates or the fitted values of the models. As an example, Figure 8A shows a plot of the within-event residuals for the regression analysis on PGA_{RotD50} with the AT3 model, while Figure 8B shows the same residuals plotted versus the fitted values, grouped for the four earthquakes considered. Figure 9 shows the same plots with reference to the calibration of the AT3 model for $SI_{H,RotD50.}$ In both cases no trends can be observed. In general, no anomalies were observed during the regression analysis. A summary of all the fitted models is provided in Table 4. Estimates of the regression parameters are provided in Annex A.

TABLE 4 Fitted attenuation models and ground motion intensity measures

IM	AT1	AT2	AT3	AT4
$Sa_{0.1-0.5}$	×	×	×	×
$I_{Mc,0.3}$	×	×	×	
$I_{Mc,0.75}$	×	×	×	
$I_{Mc,1.5}$	×	×	×	
$I_{Np,0.3}$	×	×	×	
$I_{Np,0.75}$	×	×	×	
$I_{Np,1.5}$	×	×	×	
PGA	×	×	×	×
$Sa_{avg,0.3}$	×	×	×	×
$Sa_{avg,0.75}$	×	×	×	×
$Sa_{avg,1.5}$	×	×	×	×
$Sa_{T1,0.3}$	×	×	×	×
$Sa_{T1,0.75}$	×	×	×	×
$Sa_{T1,1.5}$	×	×	×	×
$SI_{H,K,0.3}$	×	×	×	
$SI_{H,K,0.75}$	×	×	×	
$SI_{H,K,1.5}$	×	×	×	
SI_{H}	×	×	×	
$SI_{m,0.3}$	×	×	×	
$SI_{m,0.75}$	×	×	×	
$SI_{m,1.5}$	×	×	×	

As described above, for each IM, IM_{RotD0}, IM_{RotD50}, and $IM_{RotD100}$ were considered.

Figures 10 and 11 show examples of the fitted GMRSs, for PGA_{RotD50} and $SI_{H,RotD50}$, respectively. In these figures the circles indicate IM values as computed from the recordings of GMPEs, the black line indicates $\mu_{\log IM_{e,r}}$ (see Equation 2), while the red curve corresponds to $\mu_{\log(IM_{e,s})} + \delta_{B_e}$. In general, the between-event variability δ_{B_e} was very small, since all the earthquakes considered are part of the same seismic sequence. In the two examples in Figures 10 and 11, it can be noticed that the δ_{B_e} terms are almost zero for all the earthquakes considered in case of PGA_{RotD50} - the black and red curves are overlapped - while they have slightly larger values for $SI_{H,RotD50}$, in particular for the aftershocks IT-2012-0032 and IT-2012-0010. The within-event standard deviations, reported in Annex A, are small if compared to other models available in the literature,[26] because the models fitted in the present paper were calibrated using earthquakes from the same seismic sequence, which feature very similar geometric attenuation. They range from 0.25 to 0.29 for most of the models.

In order to compare the GMPEs derived here with those available in the literature, Figure 12A shows, with reference to the 29th May earthquake, the residuals for the AT3 model for $\log_{10}(PGA_{RotD50})$ and those for.[26] These latter residuals are in terms of base-10 logarithm of the maximum recorded horizontal PGA, $\log_{10}(PGA_{max})$, and were derived from the output of Shakemap 4.0 available on the INGV shakemap website.[11] The two sets of residuals are similar, suggesting similar goodness of fit for the two modes, even those for[26] are slightly biased and present more outliers, probably due to the different site effect model. It should be noticed that the bias does not affect the shakemaps because it is corrected when calculating the between-event residual (Equation 6). Finally, Figure 12B shows a comparison of the two GMPEs in terms of PGA attenuation of rock sites. It can be noticed that their main difference is in the corner distance, which is higher for AT3.

3.5 | Spatial correlation model

In this work, a spatial correlation model was derived empirically by constructing semi-variograms by analysing the residuals of the regression analyses on data from the 29th May earthquakes; in fact for the 20th May event, there is a major lack of stations in the epicentral area. The other events recorded after the 20th May event were not considered because

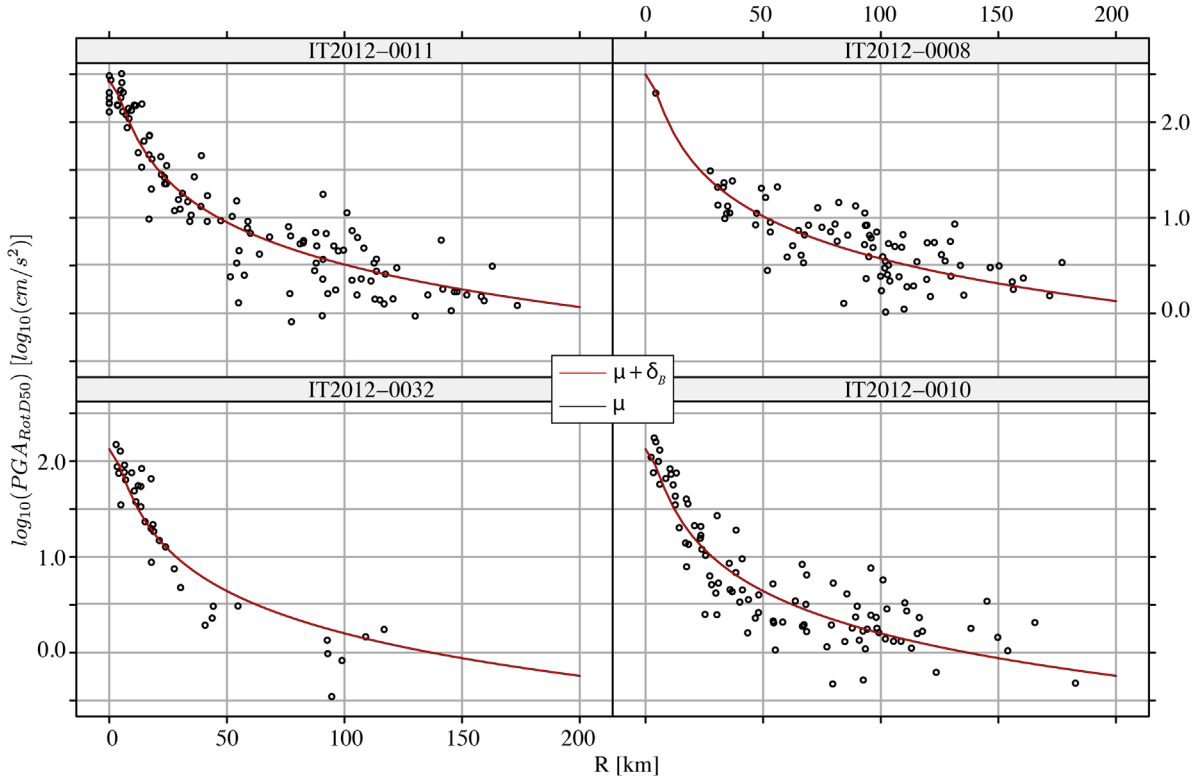

FIGURE 10 Predictions of the median value of $\log(\mathrm{PGA}_{\mathrm{RotD50}})$ by the AT3 model against Joyner-Boore distance for the different earthquake considered. Circles represent recorded IM values obtained from GMRSs.

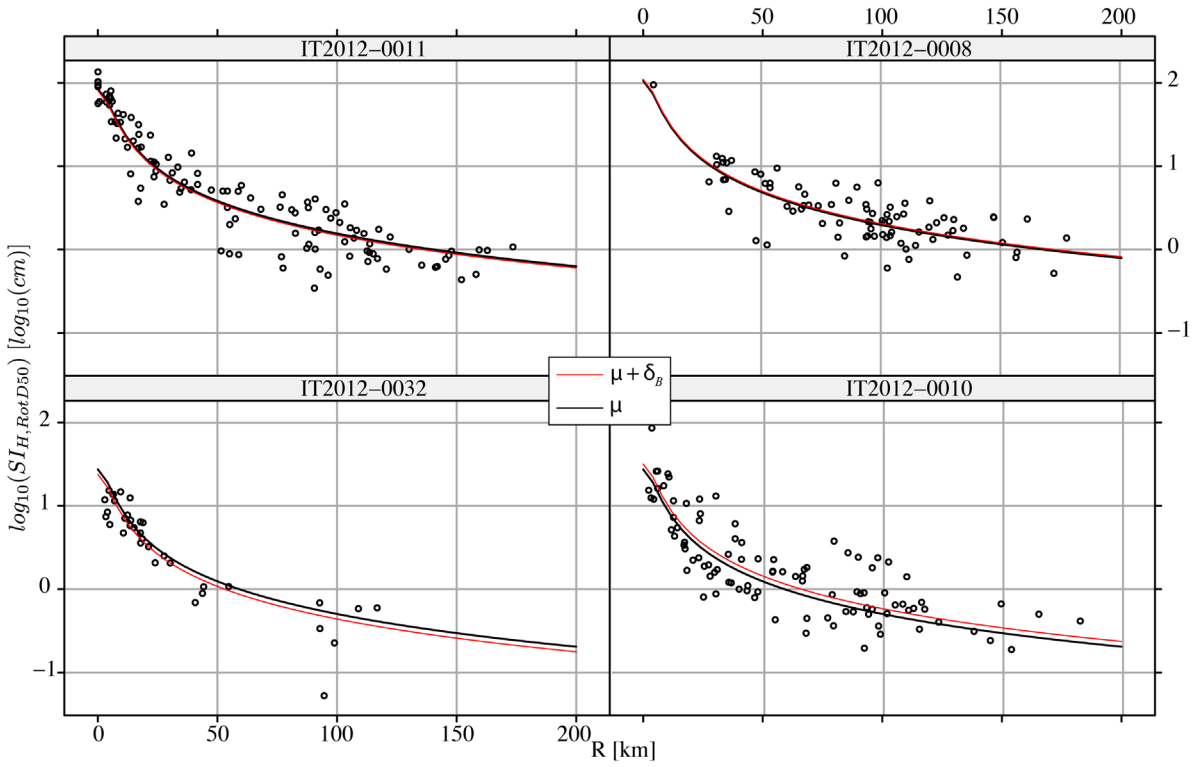

FIGURE 11 Predictions of the median value of $\log(\mathrm{SI}_{\mathrm{H,RotD50}})$ by the AT3 model against Joyner-Boore distance for the different earthquake considered. Circles represent recorded IM values obtained from GMRSs.

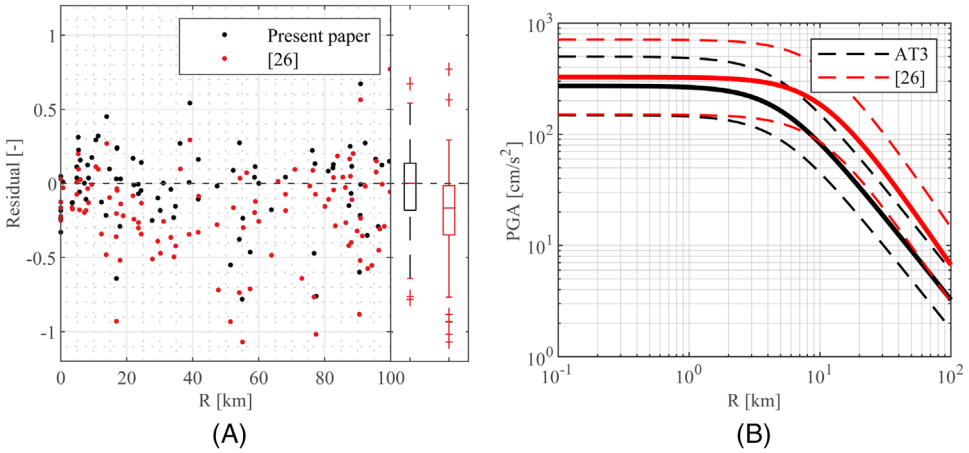

FIGURE 12 29th May 2012 Earthquake, GMPE logarithmic residuals at the GMRSs for the AT3 model and,[26] used for INGV shakemaps. PGA attenuation on rock sites according to model AT3 and,[26] used by INGV shakemaps.

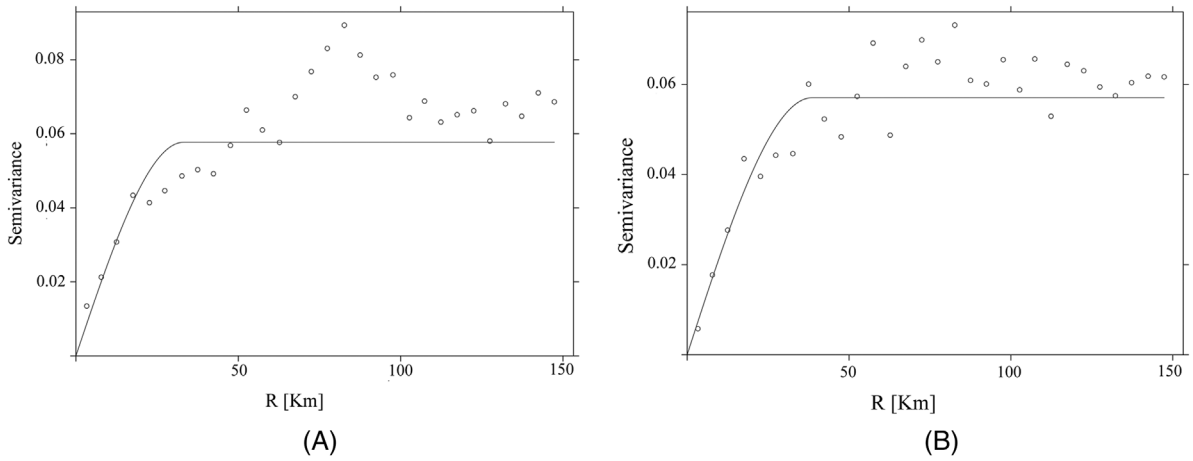

FIGURE 13 Empirical semivariograms for the attenuation model AT3 considering PGA_{RotD50} (A) and SIH_{RotD50} (B).

the main focus of the present paper is deriving IM prediction for the 20th and 29th May events, since they produced most of the damage on buildings. To this purpose the approach described by Jayaram and Baker[5] is used. After the calculation of empirical semi-variograms, different fitting models were tested; it is thought that the spherical semi-variogram model better fitted to the sample semi-variograms. This model is expressed as:

$$\gamma(h) = \begin{cases} \frac{3}{2}\frac{h}{a} - \frac{1}{2}\left(\frac{h}{a}\right)^3 & for\ 0 \le h \le a \\ 1 & for\ h > a \end{cases} \tag{30}$$

with a being the range and h the separation distance, whereas $\gamma(h)$ is the semivariance. The spatial correlation is obtained by subtracting the semivariance from unity. As an example, Figure 13 shows the semivariograms obtained from the residuals of the AT3 model for $PGA_{,RotD50}$ (Figure 13A) and $SI_{H,RotD50}$ (Figure 13B) with the corresponding fitted spherical models. The estimates of the ranges for all the spatial correlation models are reported in the Annex B. They span from a minimum of 16.81 km for $Sa_{T1,0.3,RotD100}$ (AT3 model) to a maximum of 57.70 km for $Sa_{T1,1.5,RotD0}$. In general it is observed that IM based on longer spectral period are associated to higher values of the range and that on average the range decreases passing from RotD0 values to RotD100.

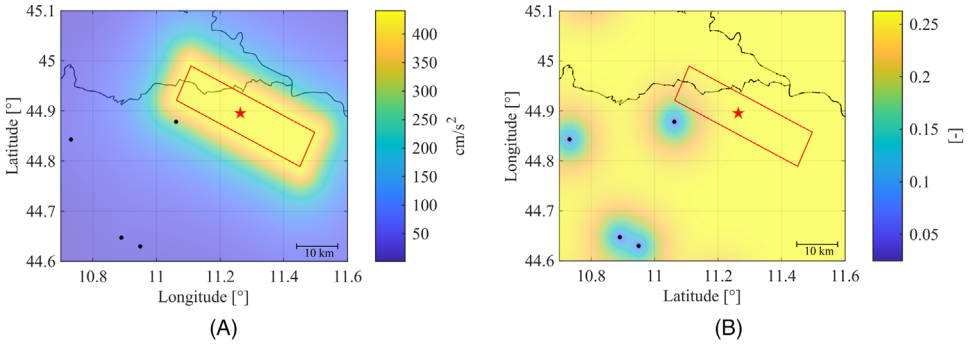

FIGURE 14 Median value (A) and logarithmic standard deviation (B) of $PGA_{,RotD50}$ produced by the 20 May mainshock, obtained using the AT3 GMPE.

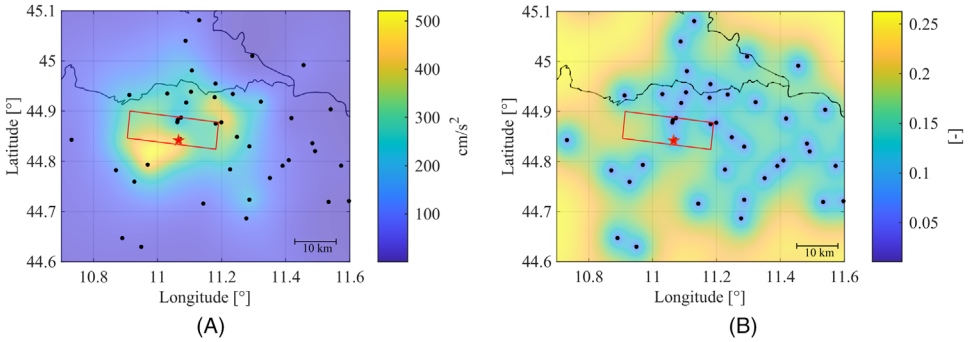

FIGURE 15 Median value (A) and logarithmic standard deviation (B) of $PGA_{,RotD50}$ produced by the 29 May mainshock, obtained using the AT3 GMPE

4 | SHAKEMAPS FOR THE EMILIA 2012 EARTHQUAKES

Shakemaps for both the 20 May and 29 May mainshocks were computed, considering all the ground motion IMs listed in Section 3.1 and the different site effect models described in Section 3.4. The procedure described in Section 2 was implemented by the authors using the Matlab programming language. Conditional IM values were computed at the points of a regular grid with a spacing of 0.009 decimal degrees. Only these two earthquakes are considered because they are the most relevant in the framework seismic fragility assessment, since they produced most of the damage on buildings.[22,47]

When using the AT2 and AT3 models, soil category C was assumed at all the grid points considered for computing the maps. This assumption is justified by the widespread diffusion of this soil class at the locations of the GMRS closer to the epicentre (see Section 3.3). The site amplification coefficient for the GMPE AT3 depends on the IM $Sa_{0.1-0.5}$ on soil class A. Therefore, a first shakemap was calculated for this IM and then its median values were used to compute the value of site effect coefficient at each grid point. The shakemaps for all the other IMs under consideration were first computed assuming soil class A and then scaled using the so obtained values of the site effect coefficient. For the maps based on the AT1 and AT4 models $V_{s,30}$ values at the grid-points were estimated using the continuum approximation models described in Section 3.3. The adopted values of $Z_{1,0}$ for the model AT4 are those reported in Figure 3. Similar to what was done for the GMPE AT3, shakemaps were first computed assuming rock site conditions and then scaled considering the values of $V_{s,30}$, and for the model AT4 the values of $Z_{1.0}$, at the different grid-points.

As examples of the shakemaps computed, Figures 14 and 15 show maps for the PGA associated to the 20 May and the 29 May mainshocks with the AT3 model, respectively, in the epicentral area of the earthquakes. Each figure shows the conditional median value of the PGA (i.e. $10^{\mu_{\log(IM_{e,s})|\log(\boldsymbol{IM}_{e,GMRS})}}$)and the corresponding conditional logarithmic standard deviation, computed as the square root of the variance estimated by Equation (10). As discussed above, at sites far from recording stations the logarithmic standard deviation tends to the within-event standard deviation of the GMPE. Clearly, the shakemap associated to the 20 May event has a higher uncertainty due to the limited number of recording stations.

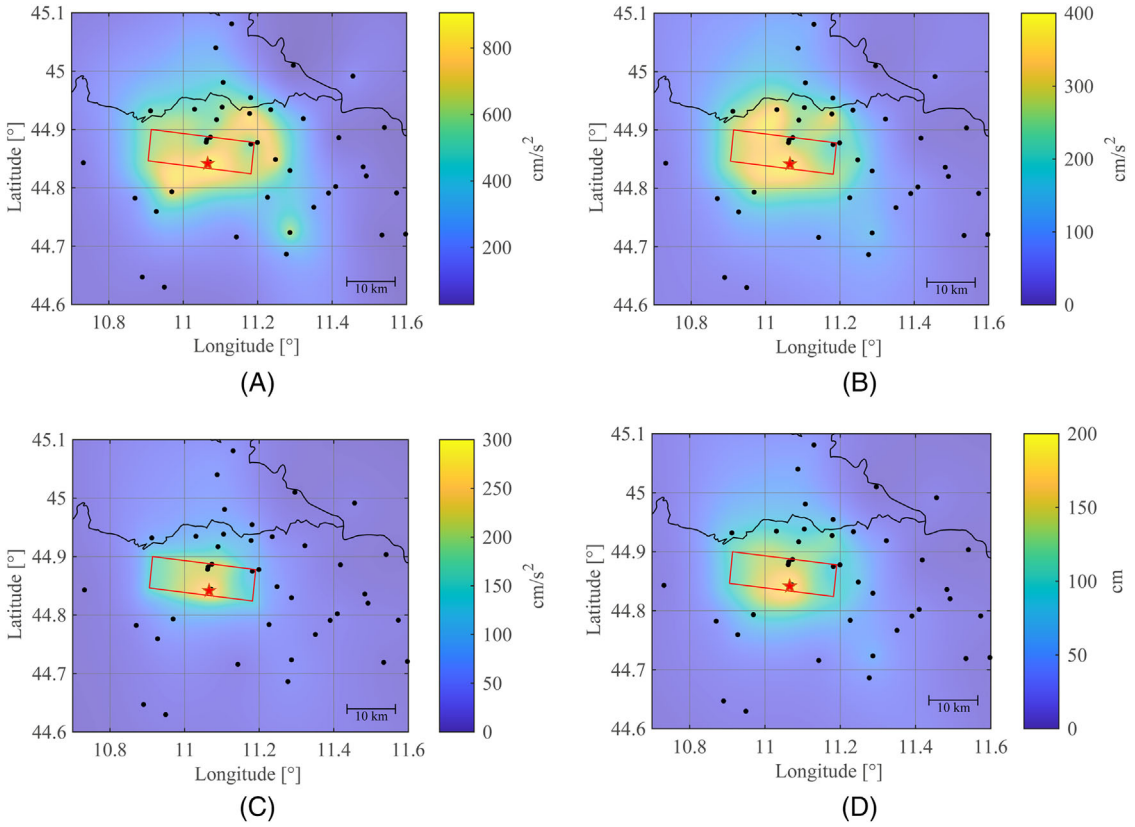

FIGURE 16 Median value of (A) $Sa_{avg,0.3,RotD50}$, (B) $Sa_{avg,0.75,RotD50}$, (C) $Sa_{avg,1.5,RotD50}$, (D) $SIH_{,RotD50}$

This highlights the importance of a dense GMRS grid in order to obtain accurate predictions of the ground-motion intensity.

With reference to the 29 May earthquake Fig. 16 shows maps in terms of $Sa_{avg,0.3,RotD50}$, $Sa_{avg,0.75,RotD50}$$Sa_{avg,0.}$,$Sa_{avg,1.5,RotD50}$ and $SIH_{,RotD50.}$ It is interesting to observe that the areas at which the highest values of the average accelerations in the different period ranges are predicted are different. The highest values of $Sa_{avg,0.3,RotD50}$ (Figure 16A) are predicted south west of the surface projection of the fault surface and close to the epicentre, high values are observed also north east of the fault area. $Sa_{avg,0.75,RotD50}$ values are high on the west of the fault area, with a peak also north west. Finally the highest $Sa_{avg,1.5,RotD50}$ and $SIH_{,RotD50}$ figures are predicted within the surface projection of the fault surface. The analysis of the correlation of the different IM values with damage data is far beyond the scope of the present paper, but studies on observational fragility analyses can benefit from the predictions provided in the present paper.

Finally, it should be noticed that it is not possible to directly compare the shakemaps presented in the present paper with those computed by INGV because they consider the maximum of the two horizontal components as IM values,[15] while in the present paper we consider rotation independent values. Furthermore, the scope of INGV maps is providing a rapid assessment of the ground motion intensity in terms of a few IMs, using general GMPEs, calibrated on data from many different earthquakes.

All the shakemaps obtained are provided if the form of tables as supplementary material to this paper.

4.1 | Analysis of the prediction error

To decide which Model provides the best estimates and should be preferred when computing the conditional ground motion distribution, it is necessary to compare the accuracy of the prediction of each map for the different IMs. At the same time, this process allows us to study the influence of the site effects term definition. To this purpose, the shakemaps computed using AT1 and AT4 models are further differentiated based on the procedure implemented

TABLE 5 Root mean square errors associated with shakemaps derived adopting the different attenuation models, listed in the first row of the table. RotD50 IM values are conside

IM	$AT1_{krig}$	$AT1_{regr}$	AT2	AT3	$AT4_{krige}$	$AT4_{regr}$
$Sa_{0.1-0.5}$[cm/s^2]	105.94	96.45	46.17	35.10	34.15	37.00
$I_{Mc,0.3}$ [cm/s^2]	91.71	90.44	45.22	37.63	x	x
$I_{Mc,0.75}$ [cm/s^2]	96.13	103.72	36.05	31.62	x	x
$I_{Mc,1.5}$ [cm/s^2]	98.98	103.09	35.42	25.30	x	x
$I_{Np,0.3}$ [cm/s^2]	89.81	101.19	47.43	37.31	x	x
$I_{Np,0.75}$ [cm/s^2]	96.45	97.08	39.21	37.31	x	x
$I_{Np,1.5}$ [cm/s^2]	110.68	123.65	39.21	21.82	x	x
PGA [cm/s^2]	96.13	134.08	46.17	33.52	34.15	34.47
$Sa_{avg,0.3}$[cm/s^2]	61.03	178.04	28.78	25.93	27.51	22.14
$Sa_{avg,0.75}$[cm/s^2]	69.57	135.35	21.50	21.50	19.92	24.35
$Sa_{avg,1.5}$[cm/s^2]	81.59	171.40	18.02	18.66	18.34	104.04
$Sa_{T1,0.3}$[cm/s^2]	69.57	111.00	25.30	25.30	25.30	28.46
$Sa_{T1,0.75}$[cm/s^2]	60.72	88.23	27.83	28.46	28.78	50.91
$Sa_{T1,1.5}$[cm/s^2]	80.32	157.80	18.66	18.66	18.97	36.05
$SI_{H,K,0.3,}$ [cm]	60.40	74.95	42.69	31.31	x	x
$SI_{H,K,0.75}$ [cm]	53.13	98.03	33.20	26.25	x	x
$SI_{H,K,1.5}$ [cm]	69.57	69.57	35.42	23.08	x	x
SI_{H} [cm]	107.83	85.07	36.05	27.20	x	x
$SI_{M,0.3}$ [cm]	67.36	74.31	37.00	25.61	x	x
$SI_{M,0.75}$ [cm]	83.80	83.17	36.37	26.25	x	x
$SI_{M,1.5}$ [cm]	118.59	111.00	35.73	23.08	x	x

to extend $V_{s,30}$ values to the area of interest and subscripts *krige* and *regr* are for this reason added to the original notation.

The following procedure is adopted to measure the accuracy of the predictions:

(i) ten GMRSs closer than 50 km from the epicentre and on C soil type are randomly selected and then removed from the recording stations list;
(ii) the conditional distribution of the IM under consideration is estimated at the locations of these stations. It is worth noticing that in this case the model described in Section 2 is applied considering as sites for the conditional IM predictions the exact locations of the removed stations, without using a regular grid;
(iii) the IM measurements for the removed stations are compared with the conditional IM predictions
(iv) points from (i) to (iii) are repeated for one hundred times and then the Root Mean Square Error (RMSE) is computed as:

$$\mathrm{RMSE} = \sqrt{\frac{1}{100 \cdot 10} \sum_{j=1}^{100} \sum_{i=1}^{10} \left(IM_{j,i} - \overline{IM_{j,i}} \right)^2} \tag{31}$$

with $IM_{i,j}$ being the general IM value obtained from a GMRS and $\overline{IM_{j,i}}$ the corresponding prediction. Given the limited number of GMRSs for the 20 May event, and the purpose of the paper, this analysis was carried out with reference to the 29 May mainshock only. The values of the RMSE, obtained for the different IMs under consideration are listed in Table 5. It can be observed that IM predictions computed with the AT3 and the AT4 $_{krige}$ models are associated to the lowest average RMSE with the second model performing slightly better than the first. The good performance of the AT4 $_{krige}$ model, however, is shadowed by its limited range of applicability, as it can be adopted to estimate only a reduced set of IMs because of the soil effect model adopted (see Section 3.4). At the same time, the predictions provided by the model

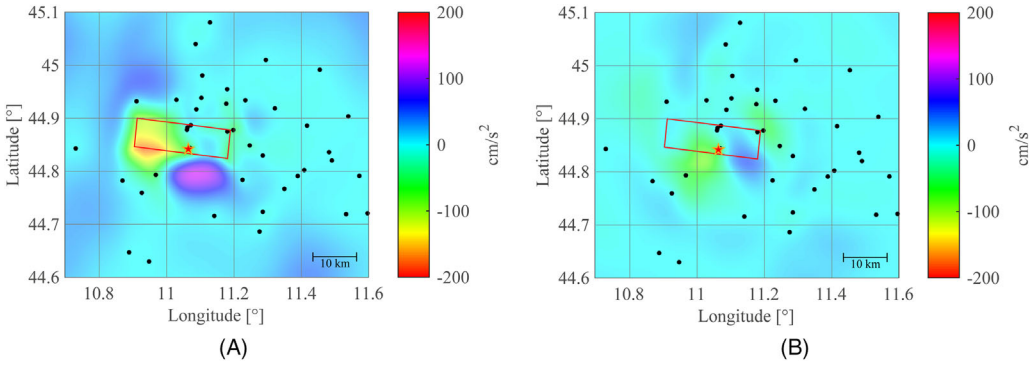

FIGURE 17 Difference in the PGA_{RotD50} predictions for the 29 May earthquake obtained using (A) the AT1 and the AT3 models and (B) the AT2 and the AT3 models. AT3 is used as reference in both cases.

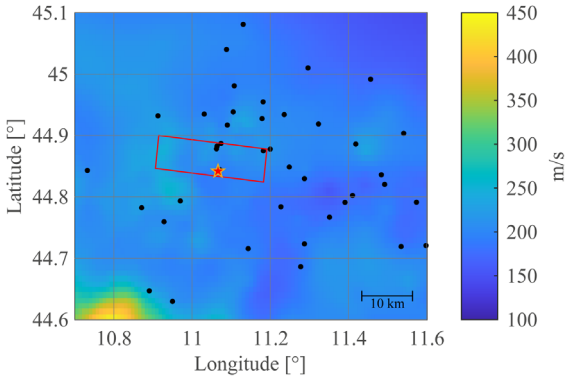

FIGURE 18 $V_{s,30}$ values predicted in the area considered for the shakemaps by the Kriging model.

AT3, which uses the non-linear soil effect model by the Italian national building code, are only slightly less accurate and cover a much wider set of IMs. Therefore, the AT3 model is to be preferred.

In order to better understand the discrepancies in the models considered, Figure 17 shows the absolute difference between the predictions of PGA_{RotD50} obtained from the $AT1_{krig}$ and the AT2 model and those from the AT3 model, used as reference. Clearly, the largest differences are observed for the $AT1_{krig}$ model which predicts lower (about 150 cm/s^2) PGA values than AT3 in the south west corner of the surface projection of the fault and higher values (about 120 cm/s^2) at the south of the fault. The differences in the case of the AT2 model are lower; at the south of the epicentre, it predicts lower PGA values (bout 90 cm/s^2), while at the south east corner of the fault surface projection it predicts higher PGA values that AT3 (about 50 cm/s^2). Since these differences cannot be justified by the variability of $V_{s,30}$ (Figure 18) they suggest that, as expected, in the near source area there are strong non-linear soil effects, which are included in AT3.

5 | CONCLUSION

The paper presented ground-motion intensity estimates for the two mainshocks of the 2021 Emilia earthquake that on the 20th and 29th May 2012 struck the provinces of Bologna, Modena and Ferrara. These maps rely on the assumption that the logarithm of any IM values over a certain area follow a multivariate normal distribution with a certain spatial correlation. Attenuation relationships and spatial correlation models have been calibrated for different IMs, computed considering directionality effects, using data from four earthquakes of the 2012 Emilia sequence. Different site effect models have been considered and compared in terms of root mean square error by contrasting shakemap predictions with recorded IM values within an iterative procedure in which some ground motion recording stations were removed from the set of those used for computing shakemaps. It was found that the lowest mean square error values were associated to the non-linear site effect model by Chiou and Youngs[45] that considers both the effects of $V_{s,30}$ and $Z_{1.0}$. Similarly low error values were

observed also for the shakemaps computed with an attenuation model based on the nonlinear site effect model proposed by the Italian National building code, based on $V_{s,30}$ only. It should be noticed that the area investigated is mainly associated to soil type C and features a quasi-uniform bedrock depth, therefore, the conclusions on the accuracy of the IM predictions related to the different site effect models may not apply to different soil types or site configurations.

ACKNOWLEDGEMENTS

The authors gratefully acknowledge the financial support of the "Agenzia per la sicurezza territoriale e la protezione civile" of the Emilia-Romagna region.

DATA AVAILABILITY STATEMENT

The data that support the findings of this study are available from the corresponding author upon reasonable request.

ORCID

Nicola Buratti https://orcid.org/0000-0002-3785-2042

REFERENCES

1. Wald DJ, Quitoriano V, Heaton TH, Kanamori H, Scrivner CW, Worden CB. TriNet "ShakeMaps": Rapid generation of peak ground motion and intensity maps for earthquakes in southern California. *Earthq Spectra* 1999;15:537–54. https://doi.org/10.1193/1.1586057
2. Bradley BA. Site-specific and spatially-distributed ground-motion intensity estimation in the 2010–2011 Canterbury earthquakes. *Soil Dyn Earthq Eng* 2014;61–62:83–91. https://doi.org/10.1016/j.soildyn.2014.01.025
3. Worden CB, Thompson EM, Baker JW, Bradley BA, Luco N, Wald DJ. Spatial and spectral interpolation of ground-motion intensity measure observations. *Bull Seismol Soc Am* 2018;108:866–75. https://doi.org/10.1785/0120170201
4. Goda K, Hong HP. Spatial correlation of peak ground motions and response spectra. *Bull Seismol Soc Am* 2008;98:354–65. https://doi.org/10.1785/0120070078
5. Jayaram N, Baker JW. Correlation model for spatially distrributed ground-motion intensities. *Earthq Eng Struct Dyn* 2009;38:1678–708. https://doi.org/10.1002/eqe
6. Esposito S, Iervolino I. PGA and PGV spatial correlation models based on European multievent datasets. *Bull Seismol Soc Am* 2011;101:2532–41. https://doi.org/10.1785/0120110117
7. Ornthammarath T, Douglas J, Sigbjörnsson R, Lai CG. Assessment of ground motion variability and its effects on seismic hazard analysis: A case study for iceland. vol. 9. 2011. https://doi.org/10.1007/s10518-011-9251-9
8. Stafford PJ, Zurek BD, Ntinalexis M, Bommer JJ. Extensions to the Groningen ground-motion model for seismic risk calculations: component-to-component variability and spatial correlation. *Bull Earthq Eng* 2019;17:4417–39. https://doi.org/10.1007/s10518-018-0425-6
9. Bommer JJ, Dost B, Edwards B, Kruiver PP, Ntinalexis M, Rodriguez-Marek A, et al. Developing a model for the prediction of ground motions due to earthquakes in the Groningen gas field. *Geol En Mijnbouw/Netherlands J Geosci* 2017;96:s203–13. https://doi.org/10.1017/njg.2017.28
10. Program UEH. ShakeMap n.d. https://earthquake.usgs.gov/data/shakemap/
11. Istituto Nazionale di Geologia e Vulcanologia. ShakeMap INGV n.d. [Accessed November 2, 2021] http://shakemap.ingv.it/shake4/
12. Michelini A, Faenza L, Lauciani V, Malagnini L. ShakeMap implementation in Italy. *Seismol Res Lett* 2008;79:688–97. https://doi.org/10.1785/gssrl.79.5.688
13. Braga F, Gigliotti R, Monti G, Morelli F, Nuti C, Salvatore W, et al. Post-seismic assessment of existing constructions: evaluation of the shakemaps for identifying exclusion zones in Emilia. *Earthquakes Struct* 2015;8:37–56. https://doi.org/10.12989/eas.2015.8.1.037
14. Worden C., Wald DJ. ShakeMap Manual Online: technical manual, user's guide, and software guide. 2020. https://doi.org/10.1234/012345678
15. Michelini A, Faenza L, Lanzano G, Lauciani V, Jozinović D, Puglia R, et al. The New ShakeMap in Italy: Progress and Advances in the Last 10 Yr. *Seismol Res Lett* 2020;91:317–333.
16. Savoia M, Buratti N, Vincenzi L. Damage and collapses in industrial precast buildings after the 2012 Emilia earthquake. *Eng Struct* 2017;137:162–80. https://doi.org/10.1016/j.engstruct.2017.01.059
17. D-Amico M, Buratti N. Observational Seismic Fragility Curves for Steel Cylindrical Tanks. *J Press Vessel Technol Trans ASME* 2019;141. https://doi.org/10.1115/1.4040137
18. Buratti N, Minghini F, Ongaretto E, Savoia M, Tullini N. Empirical seismic fragility for the precast RC industrial buildings damaged by the 2012 Emilia (Italy) earthquakes. *Earthq Eng Struct Dyn* 2017;46. https://doi.org/10.1002/eqe.2906
19. Buratti N. A comparison of the performances of various ground–motion intensity measures. 15th World Conf. Earthq. Eng. Lisbon, Port., 2012, p. 77.
20. Shome N, Cornell CA, Bazzurro P, Carballo JE. Earthquakes, records, and nonlinear responses. *Earthq Spectra* 1998;14:469–500.
21. D'Amico M, Buratti N. Observational Seismic Fragility Curves for Steel Cylindrical Tanks. *J Press Vessel Technol* 2018;141:010904. https://doi.org/10.1115/1.4040137

22. Ioannou I, Bertelli S, Verrucci E, Arcidiacono V, Rossetto T. Empirical fragility assessment of residential buildings using data from the Emilia 2012 sequence of earthquakes. *Bull Earthq Eng* 2021;19:1765–95. https://doi.org/10.1007/S10518-021-01047-7/TABLES/10
23. Rossetto T, Elnashai A. Derivation of vulnerability functions for European-type RC structures based on observational data. *Eng Struct* 2003;25:1241–63. https://doi.org/10.1016/S0141-0296(03)00060-9
24. Rossetto T, Ioannou I, Grant D, Maqsood T. Guidelines for Empirical Vulnerability Assessment, *GEM Technical Report*. 2014. https://doi.org/10.13117/GEM.VULN-MOD.TR2014.11
25. Engler DT, Worden CB, Thompson EM, Jaiswal KS. Partitioning Ground Motion Uncertainty When Conditioned on Station Data. *Bull Seismol Soc Am* 2022;112:1060–79. https://doi.org/10.1785/0120210177
26. Bindi D, Pacor F, Luzi L, Puglia R, Massa M, Ameri G, et al. Ground motion prediction equations derived from the Italian strong motion database. *Bull Earthq Eng* 2011;9:1899–920. https://doi.org/10.1007/s10518-011-9313-z
27. Boore DM, Stewart JP, Seyhan E, Atkinson GM. NGA-West2 Equations for Predicting PGA, PGV, and 5% Damped PSA for Shallow Crustal Earthquakes. *Earthq Spectra* 2014;30:1057–85. https://doi.org/10.1193/070113EQS184M
28. Bindi D, Massa M, Luzi L, Ameri G, Pacor F, Puglia R, et al. Pan-European ground-motion prediction equations for the average horizontal component of PGA, PGV, and 5 %-damped PSA at spectral periods up to 3.0 s using the RESORCE dataset. *Bull Earthq Eng* 2014;12:391–430. https://doi.org/10.1007/s10518-013-9525-5
29. Luzi L, Pacor F, Puglia R. Italian Accelerometric Archive v3.0. Istituto Nazionale di Geofisica e Vulcanologia, Dipartimento della Protezione Civile Nazionale 2019. https://doi.org/10.13127/itaca.3.0
30. Puglia R, Russo E, Luzi L, D'Amico M, Felicetta C, Pacor F, et al. Strong-motion processing service: a tool to access and analyse earthquakes strong-motion waveforms. *Bull Earthq Eng* 2018;16:2641–51.
31. Housner GW. Spectrum Intensities of Strong-Motion Earthquakes. *Symp Earthq Blast Eff Struct* 1952:20–36.
32. Bianchini M. Improved scalar intensity measures in performance-based earthquake engineering. 2008. https://doi.org/10.6092/unibo/amsacta/2455
33. Bojórquez E, Iervolino I. Spectral shape proxies and nonlinear structural response. *Soil Dyn Earthq Eng* 2011;31:996–1008. https://doi.org/10.1016/j.soildyn.2011.03.006
34. Cordova PP, Deierlein G, Mehanny S, Cornell CA. Development of a Two-Parameter Seismic Intensity 2001.
35. Kappos AJ. Sensitivity of Calculated Inelastic Seismic Response To Input Motion Characteristics. *4th US Natl Conf Earthq Eng* 1990;2:25–34.
36. Matsumura K. On the intensity measure of strong motions related to structural failures. *10th World Conf Earthq Eng* 1992;1:375–80.
37. Boore DM, Watson-Lamprey J, Abrahamson NA. Orientation-independent measures of ground motion. *Bull Seismol Soc Am* 2006;96:1502–11. https://doi.org/10.1785/0120050209
38. Mascandola C, Massa M, Barani S, Albarello D, Lovati S, Martelli L, et al. Mapping the Seismic Bedrock of the Po Plain (Italy) through Ambient-Vibration Monitoring. *Bull Seismol Soc Am* 2019;109:164–77. https://doi.org/10.1785/0120180193
39. Ministero delle Infrastrutture e dei Trasporti. Aggiornamento delle «Norme tecniche per le costruzioni». *Gazz Uff Della Repubb Ital* 2018:1–198.
40. Emilia-Romagna Region. Geognostic tests database n.d. https://ambiente.regione.emilia-romagna.it/en/geologia/cartography/webgis/banca-dati-geognostica?set_language=en
41. Wackernagel H. Universal Kriging. In: Springer Heidelberg B, editor. Multivar. *Geostatistics*, 2003. https://doi.org/10.1007/978-3-662-05294-5_38
42. Wackernagel H. Multivariate Geostatistics. *Multivar Geostatistics* 2003. https://doi.org/10.1007/978-3-662-05294-5
43. Douglas J, Edwards B. Recent and future developments in earthquake ground motion estimation. *Earth-Science Rev* 2016;160:203–19. https://doi.org/10.1016/j.earscirev.2016.07.005
44. Chiou B-J, Youngs RR. An NGA Model for the Average Horizontal Component of Peak Ground Motion and Response Spectra. *Earthq Spectra* 2008;24:173–215. https://doi.org/10.1193/1.2894832
45. Chiou BSJ, Youngs RR. Update of the Chiou and Youngs NGA model for the average horizontal component of peak ground motion and response spectra. *Earthq Spectra* 2014;30:1117–53. https://doi.org/10.1193/072813EQS219M
46. Team RC. R: A language and environment for statistical computing. *R Foundation for Statistical Computing* 2019.
47. Savoia M, Buratti N, Vincenzi L. Damage and collapses in industrial precast buildings after the 2012 Emilia earthquake. *Eng Struct* 2017;137. https://doi.org/10.1016/j.engstruct.2017.01.059

SUPPORTING INFORMATION

Additional supporting information can be found online in the Supporting Information section at the end of this article.

How to cite this article: Buratti N, Simoni E, Mazzotti C. Post-earthquake estimates of different ground motion intensity measures for the 2012 Emilia earthquake. *Earthquake Engng Struct Dyn*. 2022;1-21. https://doi.org/10.1002/eqe.3756